2024 IEEE/RSJ International Conference on Intelligent Robots and Systems (IROS)
October 14-18, 2024. Abu Dhabi, UAE

Trans-Rotor: An Active Omnidirectional Aerial-Ground Vehicle With Differential Gear Joint Transformation Mechanism

Xuankang Wu†, Haoxiang Sun†, Tong Xiao, Yanzhang Pan, Zheng Fang*

***Abstract*— Aerial-ground vehicles have shown great potential in various fields due to their superior mobility and outstanding endurance. However, most of morphing aerial-ground vehicles consider little about controllability and traversability in ground mode. We present a novel aerial-ground vehicle called Trans-Rotor. By proposing a differential gear joint, we equip Trans-Rotor with omnidirectional mobility in both air and ground mode. Besides, using a four-wheel-steering model in ground mode provides better traversability and ground flexibility. Moreover, we design mid-mode transformation for Trans-Rotor, which provides smooth and rapid mode switching. In this work, we firstly propose a novel design of an aerial-ground vehicle. Then, we propose a decoupled controller considering the four-wheel-steer model to achieve autonomous navigation of the vehicle. Comprehensive experiments and a benchmark comparison are carried out to validate the outstanding performance of the proposed system, where the system shows ground flexibility and saves energy up to more than 95%.**

I. Introduction

In recent years, unmanned aerial vehicles (UAVs) have gained significant attention in various scenarios such as wide-area reconnaissance and exploration of unknown environments, owing to their high maneuverability and hovering capabilities [1]. However, multicopters still have limitations that restrict their application range, such as payload capacity and endurance [2], especially when they need to carry relatively heavy payloads. By comparison, ground robots do not need to continuously overcome gravity and rely directly on frictional forces for propulsion, resulting in higher energy efficiency and payload capacity. Typical wheeled ground robots can achieve an endurance of 1-3 hours or even longer, while the majority of multicopters have an endurance of only 5-30 minutes [3]. However, the lower terrain traversal capability of ground vehicles limits their application range. For instance, when encountering large obstacles or environments with complex terrains, ground robots are forced to take detours, while multicopters can fly directly over them.

Based on the analysis above, it is intuitive that combining the advantages of multicopters and ground robots can significantly enhance the functionality of the system. One simple approach is to establish a collaborative system where multicopters and ground robots work together, leveraging their respective strengths. However, this kind of collaboration still fails to address the fundamental issues inherent to both platforms. For example, in situations where the system needs to navigate through highly complex terrains, ground robots are still constrained by their own kinematic limitations.

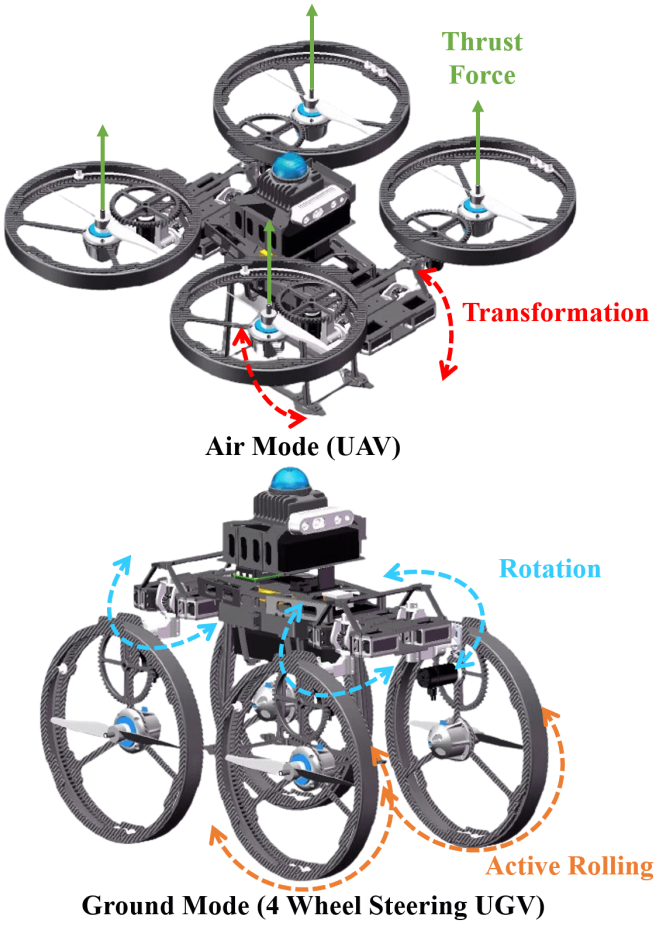

Fig. 1. Trans-Rotor: An Omnidirectional Aerial-Ground Vehicle

Another approach is to integrate the functionalities of both platforms into a single hybrid system, enabling the robot to have the capability of both aerial flight and ground locomotion. This allows the robot to conserve energy by operating on the ground when flight is not required. Additionally, such an aerial-ground robot can be applied in scenarios with restricted aerial mobility, such as pipelines, tunnels, and dense forests, thereby expanding the application range

† **Equal Contribution**

This work was supported in part by the National Natural Science Foundation of China under Grants 62073066, in part by the Fundamental Research Funds for the Central Universities under Grant N2226001, and in part by 111 Project under Grant B16009. (Corresponding author: Zheng Fang.)

The authors are all with the Faculty of Robot Science and Engineering, Northeastern University, Shenyang 110819, China. Xuankang Wu and Zheng Fang are also with the National Frontiers Science Center for Industrial Intelligence and Systems Optimization, Northeastern University, Shenyang 110819, China and and also with the Key Laboratory of Data Analytics and Optimization for Smart Industry, Ministry of Education, Northeastern University, Shenyang 110819, China. Email:{2202067, 2202058, 20208022, 20217703}@stu.neu.edu.cn, fangzheng@mail.neu.edu.cn.

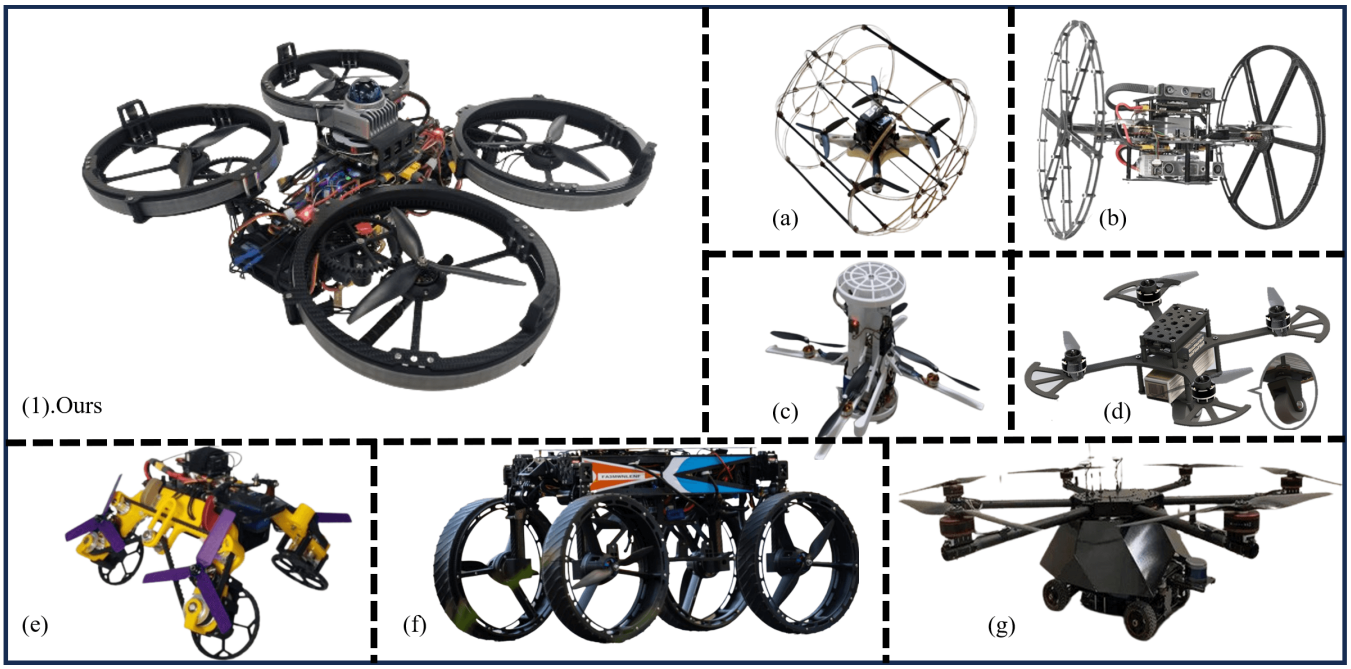

Fig. 2. Comparison of different systems. (a).Kalantari et al. [4]'s passive-cage-based vehicle. (b). Zhang et al. [5]'s passive-wheel-based vehicle. (c). Morton et al. [6]'s passive-wheel-based vehicle. (d).Pan et al. [7]'s passive-wheel-based vehicle. (e). David et al. [8]'s driving-wheel-based vehicle. (f). Sihite et al. [9]'s driving-wheel-based vehicle. (g). Tan et al. [10]'s driving-wheel-based vehicle.

of multicopters to a wider domain. A single aerial-ground robot can accomplish challenging tasks that typically require a co-operative system, such as large-scale search and rescue operations.

In previous research, various configurations of aerial-ground robots have been developed, [4]–[10], but most of them suffer from some major drawbacks, as discussed in Sec.II. In this research, building upon previous studies, we design a new aerial-ground robot called Trans-Rotor, which combines quadrotor UAV and steering wheel system. The Trans-Rotor exhibits both the flight capabilities of a conventional UAV and high flexibility of ground movement. Our system incorporates a four-wheel steering configuration, wherein each wheel possesses autonomous steering and propulsion functionalities. This architecture endows the vehicle with omnidirectional mobility, enhancing its navigational capabilities in terrestrial and aerial modes. Based on this foundation, dedicated controllers are developed for both the ground and aerial modes of operation. Comprehensive experiments are conducted to demonstrate the high energy efficiency and excellent aerial-ground locomotion capabilities of the proposed system. Finally, we compare our system with representative works featuring different configurations. The main contributions of the paper is as follows:

- A novel design of an omnidirectional aerial-ground robot based on a differential gear joint transformation mechanism is proposed, which enables the robot to operate efficiently in both aerial or ground mode.
- Decoupled controllers considering both aerial and ground operation modes are proposed to enable autonomous navigation of the robot.
- Comprehensive experimental validations are conducted to assess the control performance and power efficiency of the proposed system, and benchmark comparisons with other representative works are also carried out.

II. Related Work

A. Fixed configuration Aerial-Ground Vehicles

The conventional approach for non-deformable Unmanned Aerial Vehicles (UAVs) to achieve combined aerial-ground movement involves the addition of driven rollers or an upper-wheel drive system to the aircraft. Kalantari et al. [4] implemented a rolling cage on the periphery of the aircraft to facilitate ground movement. This cage also serves to protect the propellers during flight. However, controlling the aircraft's ground turning is challenging with this setup, as depicted in Fig. 2(a). Zhang et al. [5] added a driving wheel on both sides of the quadcopter. This configuration, however, results in relatively poor balance performance, making it difficult for the UAV to navigate and maintain balance on complex terrains, as shown in Fig. 2(b). Pan et al. [7] installed a passive wheel at the bottom of the aircraft. While this design is simple and easy to control, it fails to stabilize the UAV on the ground when the propeller is stopped. Moreover, it does not address the fundamental issue of the drone's excessive energy consumption, as illustrated in Fig. 2(d). Tan et al. [10] installed a four-wheel drive system directly on the bottom of the drone body. Although the structure is simple and easy to control, the system is bulky, leading to low flight performance, high energy consumption, and large structural size, as shown in Fig. 2(g).

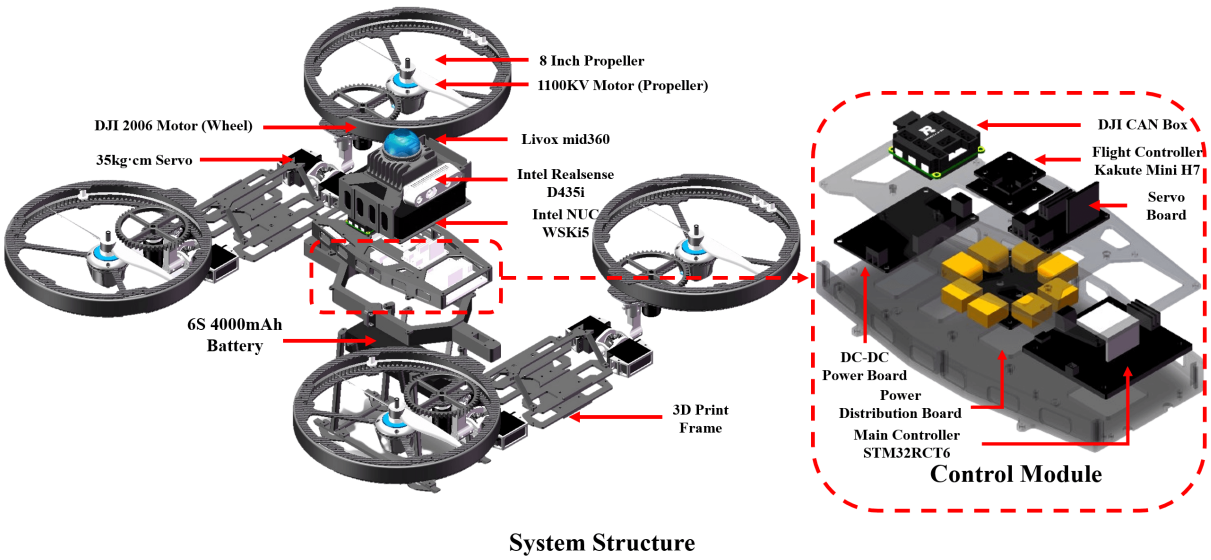

Fig. 3. Illustration of the hardware. (structural components like aluminum posts and bolts are concealed)

B. Transformable configuration Aerial-Ground Vehicles

Robots with variable configurations offer unique advantages in terms of adaptability and versatility. By incorporating the ability to transform between different modes, such as ground and aerial configurations, these robots can overcome various challenges and cross diverse environments. The flexibility of variable configuration robots enables efficient navigation through tight space, the ability to traverse rough terrain, and demonstrate higher power efficiency in ground locomotion. The small hybrid aerial-ground robot by Scott Morton et al. [6] combines ground movement and aerial flight capabilities, as illustrated in Fig. 2(c). Its key specialties include a transformation mechanism between ground and air configurations, efficient ground-based movement, the ability to overcome obstacles, and exploration of otherwise unreachable locations through air travel. Though the robot has a compact shape, its inherent structure results in limited ground traversal capabilities and payload. David et al. implement [8]the FCSTAR which does not have separate motors to rotate its wheels,as shown in Fig. 2(e). All four wheels are powered by the rear motors (which also rotate the propellers). The rotation of the front motors can be reversed to produce negative lift and increase the robot's contact force with the ground. The mechanism's transformation range from 0 to 45 degrees provides a certain level of adaptability, but this range might still be insufficient in some extreme environments or for specific tasks. A greater transformation range could allow for higher levels of terrain adaptability and the execution of more complex tasks. The Multi-Modal Mobility Morphobot (M4) by Eric Sihite et al. [9] possesses an articulated body with four propeller-driven legs that can be repurposed between thrusters, wheels and legs, as illustrated in Fig. 2(f). This modular, reconfigurable design allows the M4 to switch between flying, rolling, walking and other modes to adapt to diverse obstacles and uneven terrain. However, the robot fails to deliver satisfactory switching speeds, and the UGV mode has yet to fully exploit the characteristics of the differential mechanism to provide omnidirectional wheel motion. In contrast, our proposed Trans-Rotor has a more rapid and efficient transition process, significantly reducing the time required to switch between flying and walking modes.Besides, due to the differential gear joint, Trans-Rotor acquires omnidirectional locomotion capabilities.

III. Hardware Design

A. System Overview

As shown in Fig. 3, Trans-Rotor consists of a main chassis and four end actuators, each equipped with a wheel rim and a propeller, serving as both a wheel for ground locomotion and a thruster for aerial locomotion. The end actuators are connected to the chassis through differential gear joints, ensuring its flexibility for both ground and aerial locomotion.

Trans-Rotor comprises four DJI M2006 motor [11], four DJI C610 ESC [12], eight SPT5835W 35kg·cm 270° servos [13], four T-Motor F100 KV1100 brushless motors [14], four T-Motor F45A ESC [15], GEMFAN 8040 propellers [16], a Holybro Kakute Mini H7 flight controller [17] running PX4 firmware, a STM32F103RCT6 controller [18], and an ACE 6S 4000mAh Li-Po battery [19].

The component in an aerial mode of the Trans-Rotor is simplified by employing a quadrotor aircraft. Trans-Rotor is manufactured using 3D printing materials and has a wheelbase of 500 mm. Equipped with its robust power system, the vehicle is capable of efficiently transporting payloads exceeding 2.0 kg and attaining a ground speed of 3.0 m/s.. To ensure the safety of the propellers during deployment and retraction, the wheel rims are designed as propeller guards.

The wheel component of Trans-Rotor consists of actively driven wheels, each independently powered by a DJI M2006 motor and a DJI C610 ESC, connected to a STM32 controller via CAN communication. The steering of each wheel can be independently achieved, controlled by the differential action of two servos in the differential gear joint.

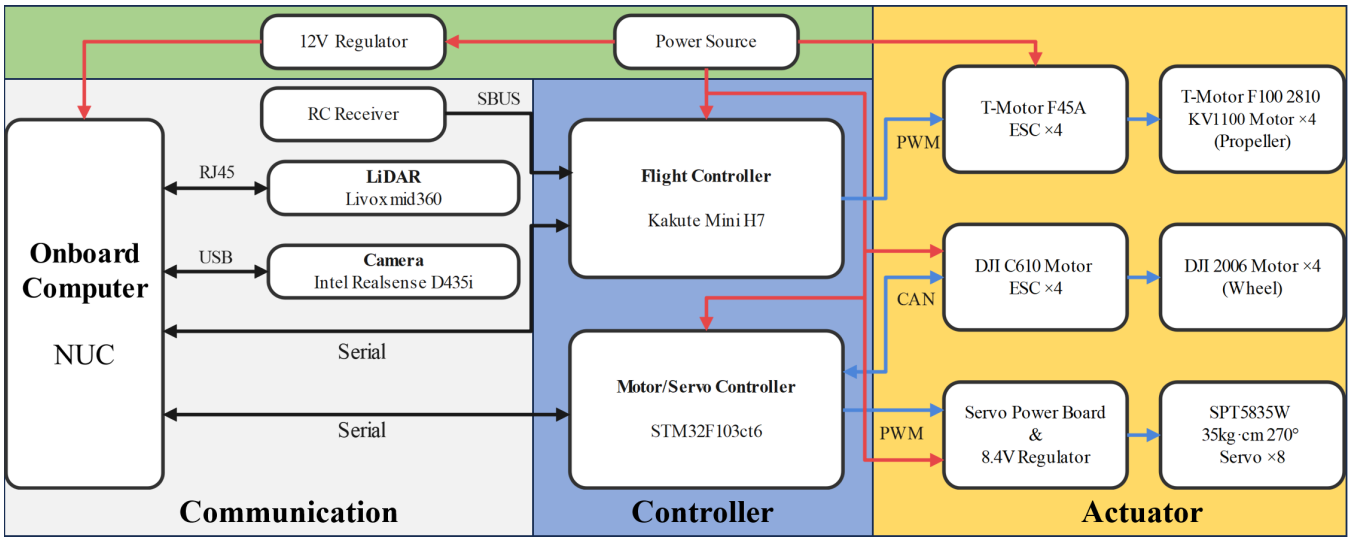

Fig. 4. Shows system electronics architecture, including the communication, controller, and power electronics components. Red lines show power connection, dark lines show data transmission, blue lines show control signal.

The onboard computer of the system is an Intel NUC WSKi5 [20], which communicates with the flight controller through MAVROS [21] to transmit IMU data and control commands. Trans-Rotor is also equipped sensors with a Livox Mid-360 LiDAR [22] and an Intel Realsense D435i depth camera [23], providing autonomous localization and perception capabilities. The weights of the various components are listed in the TABLE I below:

TABLE I
WEIGHT OF EACH COMPONENT

Component	Weight(g)
battery	530
motors & propellers & ESC	400
wheel driven motor & ESC	560
wheel	1320
servo	560
frame	720
onboard computer	235
sensor	265
aluminum posts & bolts	200
controller	60
wires	100
total	***4950***

The chassis structure of the Trans-Rotor is primarily composed of carbon fiber and 3D-printed components. The 3D printed components utilize a thermoplastic material reinforced with carbon fiber, chosen for its high strength-to-weight ratio. The system architecture of the Trans-Rotor is outlined in Fig. 4, highlighting the control systems, power electronics, and communication protocols used within the robot. The robot employs two microcontrollers for low-level motion control, one for attitude and wheel movement control, and the other for propulsor regulation.

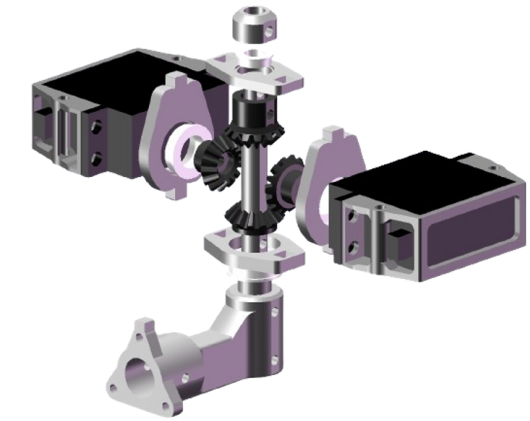

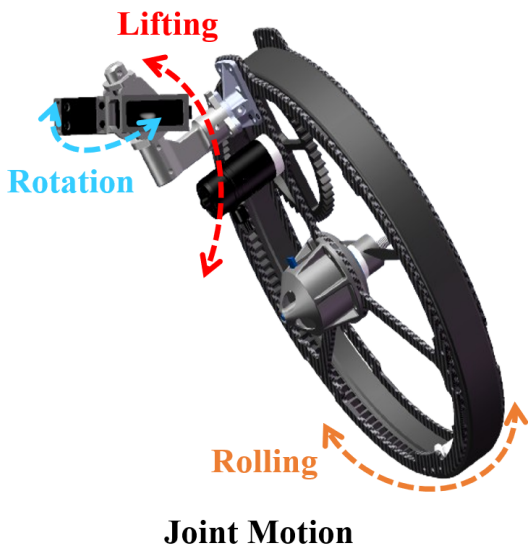

Fig. 5. The figure illustrates the motion of the differential gear joint, which consists of a set of gears and two servos.

B. Differential Gear Joint

The objective of this work is to design a multimodal robot that retains high flexibility in ground mode, while ensuring that each wheel has independent steering and propulsion capabilities. To achieve this objective, we drew inspiration from swerve drive chassis structures and differential mechanisms, leading to the design of a differential gear joint and its end-effectors, as shown in Fig. 5. Each joint consists of two servos and a pair of gears. To ensure that the differential rotation between servos maintains a consistent range of motion, all gears have a gear ratio of 1:1.

In the design, two servos are coupled in parallel to control the motion of a joint. When both servos rotate at the same speed, they act on the joint's central axis simultaneously, doubling the joint's torque to its rated value, up to 7 N·m, and facilitating the lifting motion of the joint. During differential rotation, the central axis gear rotates, resulting in the rotational movement of the joint. When the robot needs to remain stationary, we can lock the joint's position to ensure it does not deviate.

Through this design, we are able to achieve high flexibility in ground mode for the multimodal robot. Each wheel possesses independent steering and propulsion capabilities, and the design of the differential gear joint along with its terminal actuating mechanism enables precise control and stable movement of the robot across different modes of motion. The implementation of this design will offer greater flexibility and adaptability for the applications of multimodal robots.

As the motion control process described above, two servos can be coupled to control a set of joints. Combined with the propellers on the end-wheel system and the two drive motors on the wheel rims, this allows for independent drive and directional control of each end-wheel system.

IV. Kinmatic and Dynamic Models

A. Air Mode

In this work, two coordinate systems are introduced for subsequent discussions: the body coordinate system ($\mathbf{x_b}-\mathbf{y_b}-\mathbf{z_b}$) and the FLU (Front-Left-Up) world coordinate system ($\mathbf{x_w}-\mathbf{y_w}-\mathbf{z_w}$). The kinematics between each mode are considered independently, as the ground mode and aerial mode are completely decoupled. The force analysis for the aerial mode is depicted in Fig. 6.

Assuming that air resistance is negligible and that the direction of wheel motion is always aligned with the object's velocity, as the rotation of the wheels is a relatively instantaneous process, the analysis can be simplified by disregarding the robot's state during the instantaneous wheel rotation. The robot's state can be described as $x = \{\mathbf{r}, \mathbf{R}\}$, where $\mathbf{r}$ represents the position of the robot's center of mass in the world coordinate system, and $\mathbf{R}$ represents the rotation of the robot relative to the world coordinate system. The input to the system can be denoted as $u = \{f, \tau\}$, where f represents the total thrust, and τ represents the torque generated by the thrust.

The dynamic model of the aerial mode is described using the Newton-Euler equations [24]:

$$m\ddot{\mathbf{r}} = -mg\mathbf{z}_W + u_1\mathbf{z}_B, \tag{1}$$

The angular acceleration is depicted by the Euler equations:

$$\dot{\omega}_{BW} = \mathcal{I}^{-1}\left[-\omega_{BW} \times \mathcal{I}\omega_{BW} + \tau\right], \tag{2}$$

where $\mathcal{I}$ is the moment of inertia matrix with respect to the centroid along the ($\mathbf{x_b}-\mathbf{y_b}-\mathbf{z_b}$) axes. The state of the system is determined by the centroid's position and velocity, as well as its orientation (locally parameterized by Euler angles) and angular velocity:

$$\mathbf{x} = [x, y, z, \phi, \theta, \psi, \dot{x}, \dot{y}, \dot{z}, p, q, r]^T. \tag{3}$$

B. Ground Mode

The ground mode kinematics of the robot can be modeled as a system composed of four steerable wheels [25]. In the inertial coordinate system, the position of the robot's body is represented by the coordinates (x, y), and its velocity by the components (v_x, v_y). The left front wheel can be defined as LF, the right front wheel as RF, the left rear wheel as LR, and the right rear wheel as RB. The linear velocity of the body is V, and the angular velocity of the body is

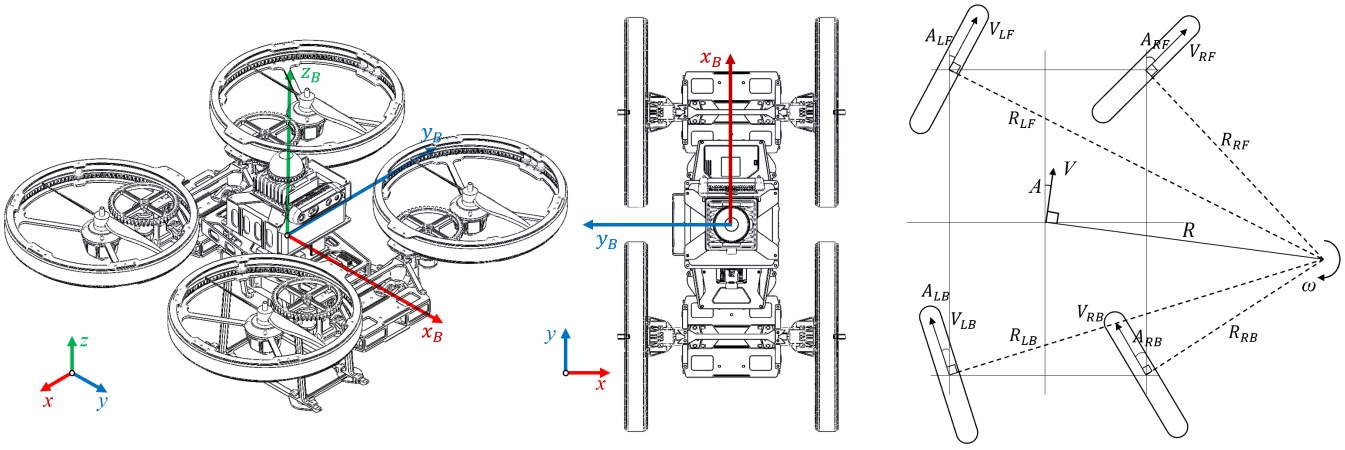

Fig. 6. Model frame definition of the proposed system.

ω. The linear velocities at the centers of the wheels are V_{LF}, V_{RF}, V_{LR}, and V_{RB}, respectively. The turning radius of the body is R, while the turning radii at the centers of the wheels are R_{LF}, R_{RF}, R_{LR}, and R_{RB}, respectively. The angle between the linear velocity and the body is A, and the yaw angles at the centers of the wheels are A_{LF}, A_{RF}, A_{LR}, and A_{RB}, respectively. The distance between the front and rear axle of the steerable wheels is L, and the distance between the left and right wheels is W. Under the ground mode, the controller is directly controlling the robot's velocity and angular velocity, i.e., $[v_x, v_y, \omega]$, and based on physical relations, the following equations can be derived:

$$V = \sqrt{V_x^2 + V_y^2}, \tag{4}$$

$$R = \frac{V}{\omega}, \tag{5}$$

$$A = \arctan \frac{V_y}{V_x}, \tag{6}$$

Based on the geometric relations, the following equations can be deduced:

$$\begin{aligned}
R_{LF} &= \sqrt{\left(\frac{L}{2} + R\sin A\right)^2 + \left(\frac{W}{2} + R\cos A\right)^2}, \\
R_{LB} &= \sqrt{\left(\frac{L}{2} - R\sin A\right)^2 + \left(\frac{W}{2} + R\cos A\right)^2}, \\
R_{RF} &= \sqrt{\left(\frac{L}{2} + R\sin A\right)^2 + \left(R\cos A - \frac{W}{2}\right)^2}, \\
R_{RB} &= \sqrt{\left(\frac{L}{2} - R\sin A\right)^2 + \left(R\cos A - \frac{W}{2}\right)^2},
\end{aligned} \tag{7}$$

Based on the equations above, the control parameters can be expressed as follows:

$$\begin{aligned}
V_{LF} &= R_{LF} \cdot \omega, \\
V_{LB} &= R_{LB} \cdot \omega, \\
V_{RF} &= R_{RF} \cdot \omega, \\
V_{RB} &= R_{RB} \cdot \omega,
\end{aligned} \tag{8}$$

$$\begin{aligned}
A_{LF} &= \arctan \frac{\frac{L}{2} + R\sin A}{R\cos A + \frac{W}{2}}, \\
A_{LB} &= \arctan \frac{\frac{L}{2} - R\sin A}{R\cos A + \frac{W}{2}}, \\
A_{RF} &= \arctan \frac{\frac{1}{2} + R\sin A}{R\cos A - \frac{W}{2}}, \\
A_{RB} &= \arctan \frac{\frac{1}{2} - R\sin A}{R\cos A - \frac{W}{2}},
\end{aligned} \tag{9}$$

Combining the robot's state, wheel rotation speed, and wheel steering angle, there are 11 state variables in total to represent the position and orientation of the mobile robot:

$$\mathbf{x} = [x, y, \theta, V_{LF}, V_{LB}, V_{RF}, V_{RB}, A_{LF}, A_{LB}, A_{RF}, A_{RB}]^T. \tag{10}$$

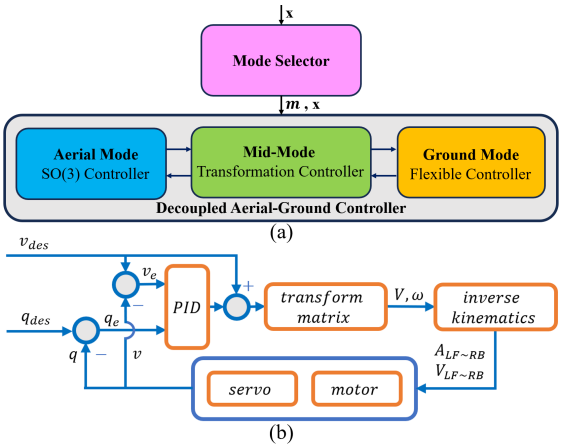

Fig. 7. Illustration of Controller Design on Trans-Rotor (a) and Gound Mode Controller Design (b).

V. Decoupled Aerial-Ground Controller Design

As Trans-Rotor cannot simultaneously engage in aerial and terrestrial modes, the control system is decoupled designed. However, it is essential to incorporate transitional modes to facilitate switching between these two modes. In this system, we designed a decoupled aerial-ground controller for Trans-Rotor which is shown in Fig.7(a).

The mode selector accepts robot state x and sends proper robot mode m and state x to controller. Mid-Mode is used for decoupled mode transformation.

In the aerial mode, the dynamics described in Sec. IV conform to the conventional quadrotor drone model. Mature drone controller SO(3) [26] is applied in aerial mode.

For ground mode, it is necessary to design an independent controller tailored to the four-steered-wheel model [27]. For terrestrial target trajectory tracking, the robot's tracking objective is defined as the desired position q_{des} = [x,y,θ] with the primary goal being to minimize the error between the robot and the target position. The design of the controller is illustrated in Fig. 7(b).

The rotation matrix from the body coordinate system to the world coordinate system R_{WB} can be expressed as follows:

$${}^{W}R_B = \begin{bmatrix} \cos\theta & -\sin\theta & 0 \\ \sin\theta & \cos\theta & 0 \\ 0 & 0 & 1 \end{bmatrix}, \tag{11}$$

$${}^{B}R_W = {}^{W}R_B^{\top}, \tag{12}$$

The position errors and velocity errors in the matrix of the body are:

$${}^{W}q_e = q_{\text{des}} - q, \tag{13}$$

$${}^{I}V_e = V_{\text{des}} - V, \tag{14}$$

$${}^{B}q_e = {}^{B}R_W {}^{W}q_e, \tag{15}$$

$${}^{B}V_e = {}^{B}R_W \cdot {}^{W}V_e, \tag{16}$$

Based on the inverse kinematic model of the chassis, with the input u being [v_x,v_y,ω], the kinematic control law for the robot in ground mode can be expressed as follows:

$$u = k_q \cdot {}^{B}q_e + k_v \cdot {}^{B}V_e + {}^{B}R_W \cdot v_{\text{des}}. \tag{17}$$

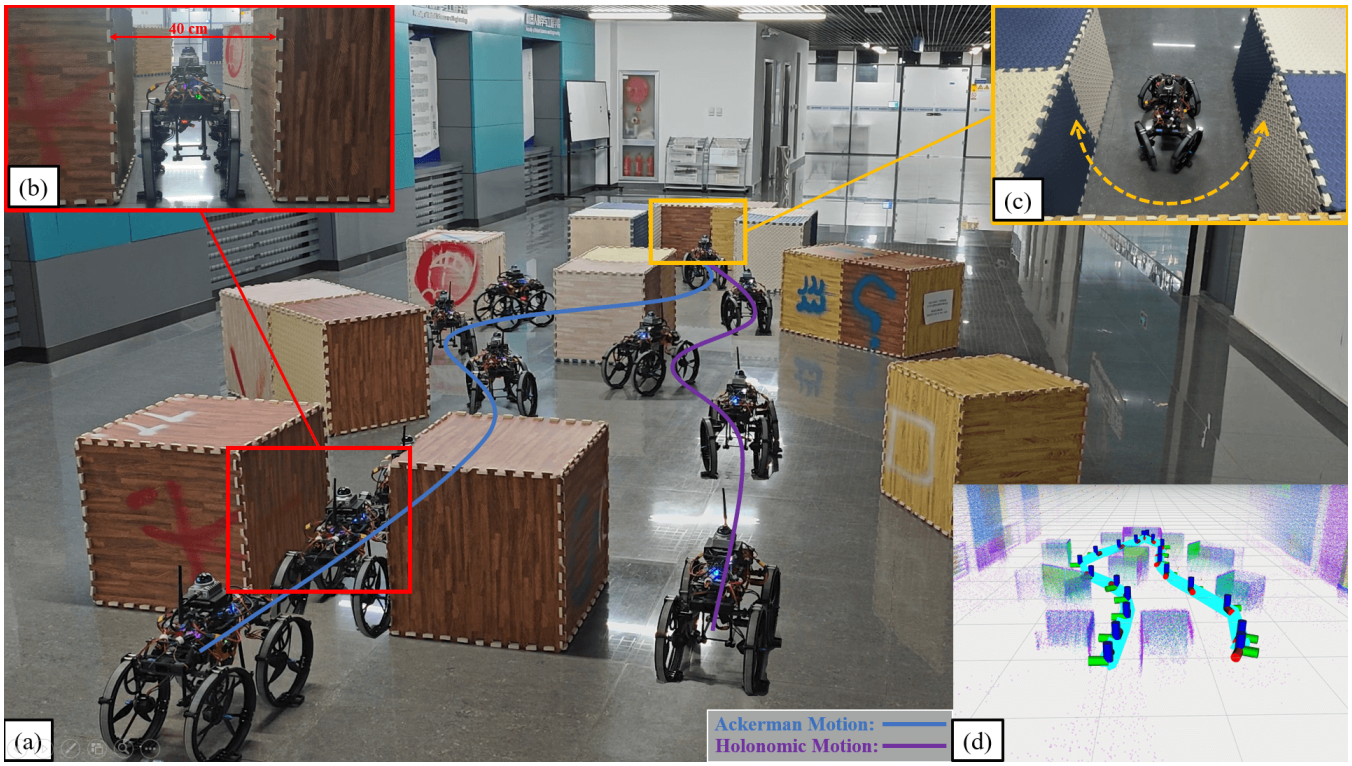

Fig. 8. Ground Locomotion Experiment

VI. Experiment

In this section, we validate the control performance, mode-switching ability, and power efficiency of the proposed system with comprehensive experiments, and carry out a benchmark comparison against other representative works of different configurations of aerial-ground vehicles.

A. Ground Locomotion Expriment

In this experiment, we have the vehicle execute a ground trajectory, where the waypoint is given by a remote controller. The maximum velocity is 2.0 m/s, the average velocity is 1.6 m/s.

The result is shown in Fig.8. Trans-Rotor's Narrow space passing ability is shown in Fig.8(b). Fig.8(c) shows Trans-Rotor's ground flexibility, which can turn in place. Fig.8(d) shows the odometry and path of robot in this experiment. We can see the vehicle can conduct smooth ground locomotion.

B. Hybrid Locomotion Expriment

We have the vehicle execute a hybrid trajectory to fly over an 0.8 m high obstacle, where the waypoint is given by a remote controller. The maximum velocity is 1.8 m/s, the average velocity is 1.0 m/s. The time duration of different mode is about 1.0 second.

The result is shown in Fig.9, which shows good hybrid locomotion. In Fig.9(b), the odometry and path of robot in this experiment are shown. Fig.9(c1)-(c4) shows Trans-Rotor's mode transformation process, which is from ground mode to air mode. While Fig.9(c4)-(c7) shows the reverse transformation process. These two transformation processes are attributed to Mid-Mode in the Trans-Rotor system.

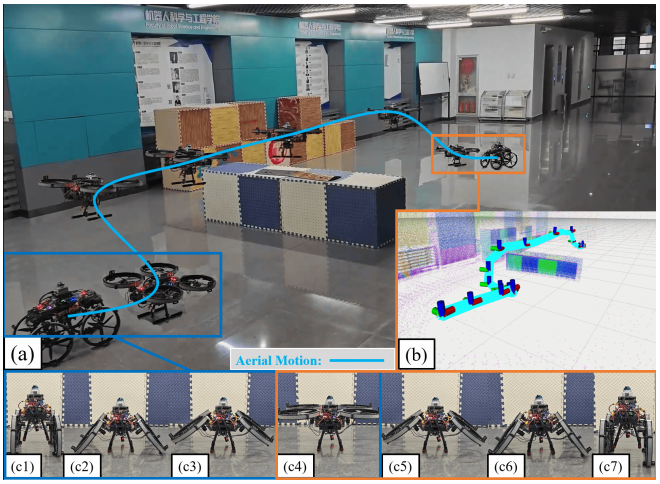

Fig. 9. Hybrid Locomotion Experiment.

C. Efficiency Validation

In this experiment, we test Trans-Rotor in ground mode by using a remote controller giving control command, which make it move in an average velocity of 1.5 m/s for 300 seconds. Power test in air mode is done by using a remote controller to control the Trans-Rotor hovering at a height about 0.8 m for 120 seconds. By measuring the energy of battery, we know that the power of aerial locomotion mode P_a is 1865 W, and the power of ground locomotion mode P_g is 76 W. In addition, we measured the standby power P_s of the vehicle, including the onboard computer, flight controller, and other components, which is 48 W. Therefore, we have the corrected power-saving efficiency:

$$\eta = (1 - \frac{P_g - P_s}{P_a - P_s}) \times 100\% = 98.5\%. \quad (18)$$

D. Benchmark Comparison

We compared the proposed system with other representative works of different configurations, namely [5], [7], [9], [10]. For better comprehensiveness, we benchmark the following performance metrics:

TABLE II: The table of the benchmark.

: Best : Worst

	Proposed	Eric et al.[9]	Pan et al.[3]	Tan et al.[4]	Zhang et al.[6]
Motion Ability	3.0m/s	2.2m/s	5.0m/s	3.0m/s	1.2m/s
Switching Speed	≈1.0s	≈2.1s	≈0s	≈5.0s	≈1.0s
Kinetic Constraint	None	Nonholonomic	None	Nonholonomic	Nonholonomic
Energy Efficiency	>95%	>95%	75.2%	58.3%	85.7%

1) **Motion ability**: this is evaluated by the fastest hybrid trajectory the vehicle can track, the faster, the better.
2) **Switching speed**: this is evaluated by the average time of mode switching, the shorter, the better.
3) **Kinetic constraint**: this is evaluated by the kinetic constraints of the vehicle's ground locomotion mode, the less, the better.
4) **Energy efficiency**: this is evaluated by the energy that the vehicle can save under ground locomotion mode with respect to aerial locomotion mode according to Eq.(18), the bigger, the better.

The result is shown in Table II. From the result, we can see that, while other works all suffer from some major drawbacks, the proposed system enjoys the energy efficiency, kinetic freedom and performs well in other places.

VII. Conclusion

In this work, we firstly propose the hardware design of novel configuration joint based on differential gear and multiple servos. We designed the Trans-Rotor, which is an active omnidirectional aerial-ground vehicle system based on differential gear joint. Further. we consider the dynamic model and kinetic model of Trans-Rotor in different mode. Later, a decoupled controller for aerial-ground locamotion is proposed. Afterward we conduct comprehensive experiments to validate the performance and the efficiency of different locomotion modes. Finally, a benchmark comparison against other representative works is conducted to reveal that the proposed system shows great performance in some perspectives while showing few demerits.

References

[1] Q. Quan, *Introduction to multicopter design and control*. Springer, 2017.

[2] L. Quan, L. Han, B. Zhou, S. Shen, and F. Gao, "Survey of uav motion planning," *IET Cyber-systems and Robotics*, vol. 2, no. 1, pp. 14–21, 2020.

[3] X. Dai, Q. Quan, J. Ren, and K.-Y. Cai, "An analytical design-optimization method for electric propulsion systems of multicopter uavs with desired hovering endurance," *IEEE/ASME Transactions on Mechatronics*, vol. 24, no. 1, pp. 228–239, 2019.

[4] A. Kalantari and M. Spenko, "Design and experimental validation of hytaq, a hybrid terrestrial and aerial quadrotor," in *2013 IEEE International Conference on Robotics and Automation(ICRA)*. IEEE, 2013, pp. 4445–4450.

[5] R. Zhang, Y. Wu, L. Zhang, C. Xu, and F. Gao, "Autonomous and adaptive navigation for terrestrial-aerial bimodal vehicles," *IEEE Robotics and Automation Letters*, vol. 7, no. 2, pp. 3008–3015, 2022.

[6] S. Morton and N. Papanikolopoulos, "A small hybrid ground-air vehicle concept," in *2017 IEEE/RSJ International Conference on Intelligent Robots and Systems (IROS)*. IEEE, 2017, pp. 5149–5154.

[7] N. Pan, J. Jiang, R. Zhang, C. Xu, and F. Gao, "Skywalker: A compact and agile air-ground omnidirectional vehicle," *IEEE Robotics and Automation Letters*, vol. 8, no. 5, pp. 2534–2541, 2023.

[8] N. B. David and D. Zarrouk, "Design and analysis of fcstar, a hybrid flying and climbing sprawl tuned robot," *IEEE Robotics and Automation Letters*, 2021.

[9] E. Sihite, A. Kalantari, R. Nemovi, A. Ramezani, and M. Gharib, "Multi-modal mobility morphobot (m4) with appendage repurposing for locomotion plasticity enhancement," *Nature communications*, vol. 14, no. 1, p. 3323, 2023.

[10] Q. Tan, X. Zhang, H. Liu, S. Jiao, M. Zhou, and J. Li, "Multimodal dynamics analysis and control for amphibious fly-drive vehicle," *IEEE/ASME Transactions on Mechatronics*, vol. 26, no. 2, pp. 621–632, 2021.

[11] DJI Inc., "Dji inc., RoboMaster M2006 P36," 2024, https://www.robomaster.com/zh-CN/products/components/general/M2006, Last accessed on 2024-3-11.

[12] ——, "Dji inc., RoboMaster C610," 2024, https://www.robomaster.com/zh-CN/products/components/general/M2006, Last accessed on 2024-3-11.

[13] SPT-Servo Inc., "Spt-servo inc., SPT5835W," 2024, http://www.spt-servo.com/Product/9516083621.html, Last accessed on 2024-3-11.

[14] T-motor Inc., "T-motor inc., T-motor F100," 2024, https://uav-cn.tmotor.com/html/2021/Motor_0910/885.html, Last accessed on 2024-3-11.

[15] ——, "T-motor inc., T-motor F45A," 2024, https://uav-cn.tmotor.com/html/2018/ESC_0712/173.html, Last accessed on 2024-3-11.

[16] Gemfanhobby Inc., "Gemfanhobby inc., Gemfan Cinelifter 8040-3," 2024, https://www.gemfanhobby.com/show.aspx?id=361&cid=73, Last accessed on 2024-3-11.

[17] Holybro Inc., "Holybro inc., Holybro Kakute H7 Mini Stacks," 2024, https://holybro.com/products/kakute-h7-mini-stacks?variant=42940542746813, Last accessed on 2024-3-11.

[18] OskarWei, "Tank dual, Available online," 2023, https://gitee.com/OskarWei/Tank_Dual, Last accessed on 2024-3-11.

[19] Grepow Inc., "Grepow inc., Grepow battery," 2024, https://www.grepow.cn/, Last accessed on 2024-3-11.

[20] Intel Corporation., "Intel ® nuc ™, Intel NUC WSKi5," 2024, https://www.intel.cn/content/www/cn/zh/products/docs/boards-kits/nuc/mini-pcs/nuc-12-pro.html, Last accessed on 2024-3-11.

[21] mavlink, "Mavros, Available online," 2014, https://github.com/mavlink/mavros, Last accessed on 2024-3-11.

[22] Livoxtech Inc., "Livoxtech inc., Livox Mid-360," 2024, https://www.livoxtech.com/cn/mid-360, Last accessed on 2024-3-11.

[23] Intel Corporation., "Intel ® realsense ™, Depth Camera D435i," 2024, https://www.intelrealsense.com/depth-camera-d435i, Last accessed on 2024-3-11.

[24] D. Mellinger and V. Kumar, "Minimum snap trajectory generation and control for quadrotors," in *2011 IEEE International Conference on Robotics and Automation*, 2011, pp. 2520–2525.

[25] T.-H. Li and M.-H. Lee, "Kinematics, dynamics and control design of 4wis4wid mobile robots," *The Journal of Engineering*, vol. 2015, 01 2014.

[26] Y. Yu, S. Yang, M. Wang, C. Li, and Z. Li, "High performance full attitude control of a quadrotor on so (3)," in *2015 IEEE International Conference on Robotics and Automation (ICRA)*. IEEE, 2015, pp. 1698–1703.

[27] P. Hang and X. Chen, "Towards autonomous driving: Review and perspectives on configuration and control of four-wheel independent drive/steering electric vehicles," in *Actuators*, vol. 10, no. 8. MDPI, 2021, p. 184.